
New Folder Name Cryo Pump Infrared

Shielding Considerations

T950087

DCC

CALIFORNIA INSTITUTE OF TECHNOLOGY
Laser Interferometer Gravitational Wave Observatory (LIGO) Project

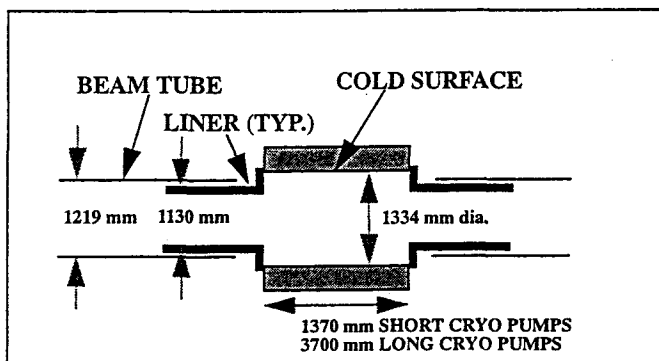
To: Distribution
From: Dennis Coyne DC
Phone/FAX: 395-2034/304-9834
Refer to: LIGO-T950087-00-E
Date: 18 Nov 95

Subject: Cryopump Infrared Shielding Considerations

Background

PSI has proposed¹ to reduce the heat load (and LN₂ consumption rate) of the cryopumps through the use of cylindrical liners (shields) with low emissivity ($\epsilon = 0.06$), diffuse surfaces on both sides of the cold surface, as indicated in Figure 1. PSI's calculations indicated a reduction in heat load to the cold surface of the long cryopump of approx. 33% is possible by using 1.52 m long liners on both sides of the long cryopump. The reduction in heat load is important in reducing the frequency of LN₂ tank refilling, reducing the size and expense of the LN₂ tank and reducing the cost of LN₂ during operation.

Figure 1: Cryopump Liners (Shields)



The "long" cryopumps have a 3.7 m long cylindrical cold surface and the "short" cryopumps have a 1.37 m long cylindrical cold surface. The internal diameters of the cold surfaces of both pumps are 1.334 m. PSI's current cryo pump design constrains the maximum diameter of the liners to be 1.13 m (PSI drawing V049-4-004, Rev. P1). The lengths of the liners for the cryo pumps are constrained by the placement of the adjacent gate valves; There appears to be some freedom in locating these gate valves relative to the cryo pump so as to achieve liner lengths on the order of 1 to 2 meters in length.

1. Process Systems International (PSI), LIGO Vacuum Equipment Preliminary Design, Vol. 1, Attachment 1.4, "80K Pump Performance", PSI-VE001AA1A01, 19 Jun 95.

Cryopump Infrared Shield Performance Analysis

An independent analysis of the effectiveness of the cryopump liner was undertaken due to concerns about the validity of two assumptions by PSI:

- 1) the entire beam tube (including the tube in proximity to the shield) acts like a black body, and
- 2) one can obtain a surface which behaves like a diffuse (Lambertian) IR reflector with low emissivity

The Lambertian characteristic of the surface is crucial; If the surface behaved as a specular reflector, then it would in essence simply mirror the black body of the beam tube to the cold surface and it would have no effect.

As reported previously¹, a view factor and radiation balance calculation² confirmed PSI's calculations of the mitigation in radiative heat load to the cold surface due to diffusive, low emissivity liners with the following parameters:

- 1) long cryopump (3.7 m cold surface length, and 1.2 m diameter³)
- 2) beam tube emissivity of 0.5
- 3) liner emissivity of 0.06 (diffuse)
- 4) liner length of 1.52 m

These calculations were based upon view factors for a coarse discretization of the geometry (i.e. a single view factor for each component). The calculations confirm that the simplification of treating the beam tube as a black body is reasonable.

Further calculations have determined the effectiveness of the liners for the revised cryo pump diameter with a finer discretization to account for the gradient in radiosity. In the analysis the geometry of Figure 1 was approximated by assuming that the beam tube, liners and cryopump cold surface are all at the same diameter (the diameter of the beam tube, 1.2 m). The analysis will be updated for a subsequent revision of this memorandum: I did not want to delay release of this memo and the discussion which will ensue of the implications of the integration of the liner and laser light baffles. In addition, the analysis does not account for the interaction of the liners with the laser light baffles (to be discussed in the next section). On the basis of this analysis, the performance of the infrared shields for the long and short cryopumps as a function of shield length and parameterized by shield emissivity, are given in Figures 2 and 3 respectively. Although the performance will change somewhat when the diameters are revised, the results will not be substantially different.

Further extension to the radiative transport analysis of the liner effectiveness to account for the different diameters of the tube, liner and cold surface as well as inclusion of the laser light baffles, can be accomplished readily. As an alternative which would permit analysis of more complex geometries, I attempted to use the TMG module within the I-Deas Master Series 2 computer aided

-
1. Coyne, D., "Cryo Pump Shield Performance Analysis", e-mail to M. Zuker, A. Lazzarini and J. Worden, 2 Nov 95.
 2. Siegel, H. and Howell, J., Thermal Radiation Heat Transfer, 2nd ed., McGraw Hill, 1972, pp.236-248.
 3. The diameter of the cryopumps was 1.2 m at the time of PSI's initial PDR (June 95). The diameter has since been increased to 1.334 m based upon laser light baffling requirements as discussed in LIGO-L950593-01-E.

design and analysis package for analysis of specular as well as diffuse components of reflection. Although TMG is capable of handling combined diffuse and forward specular reflections which are independent of incidence angle, TMG cannot handle retro-reflection. Given that suitable nearly Lambertian surfaces are obtainable (as discussed in the next section), TMG may be adequate for any further analysis with more complex geometry (if necessary). Inclusion of a complete BRDF characterization in the analysis would require another code, perhaps TRASYS or CODE-V.

**Figure 2: Long Cryopump Liner (Infrared Shield) Performance
(for liner emissivities of 0.06 and 0.10)**

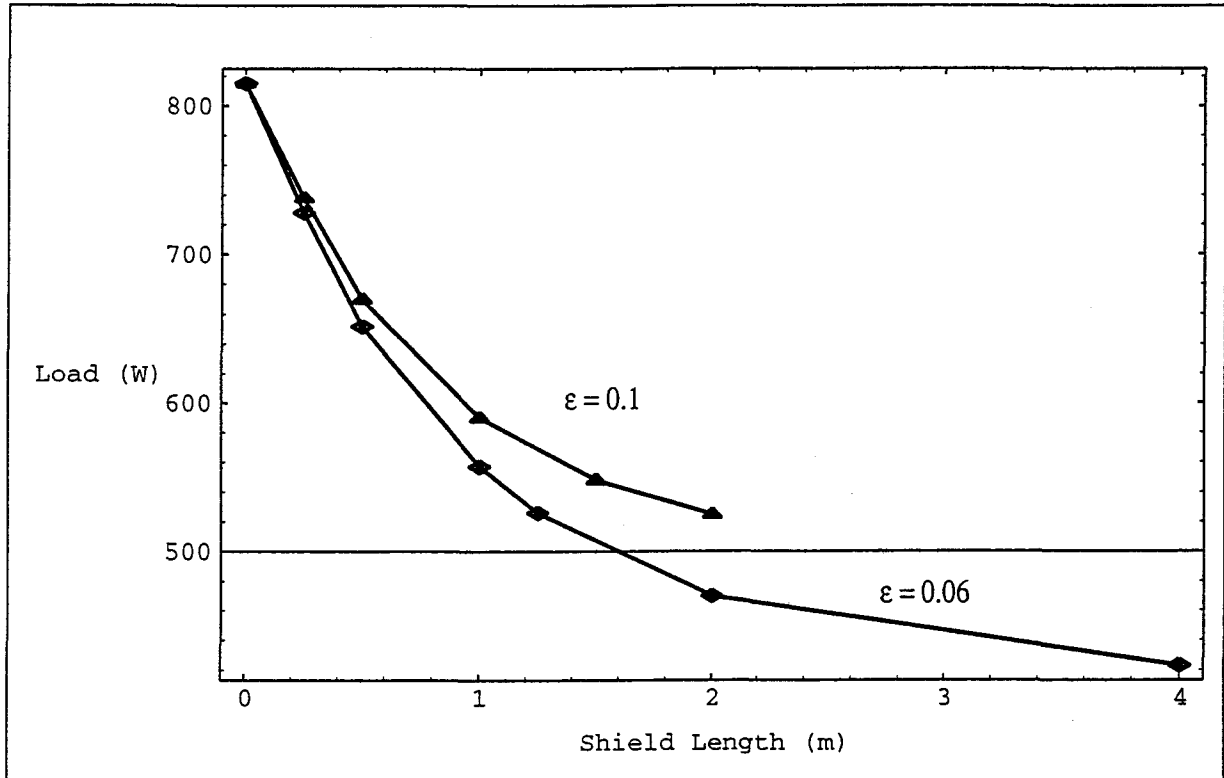
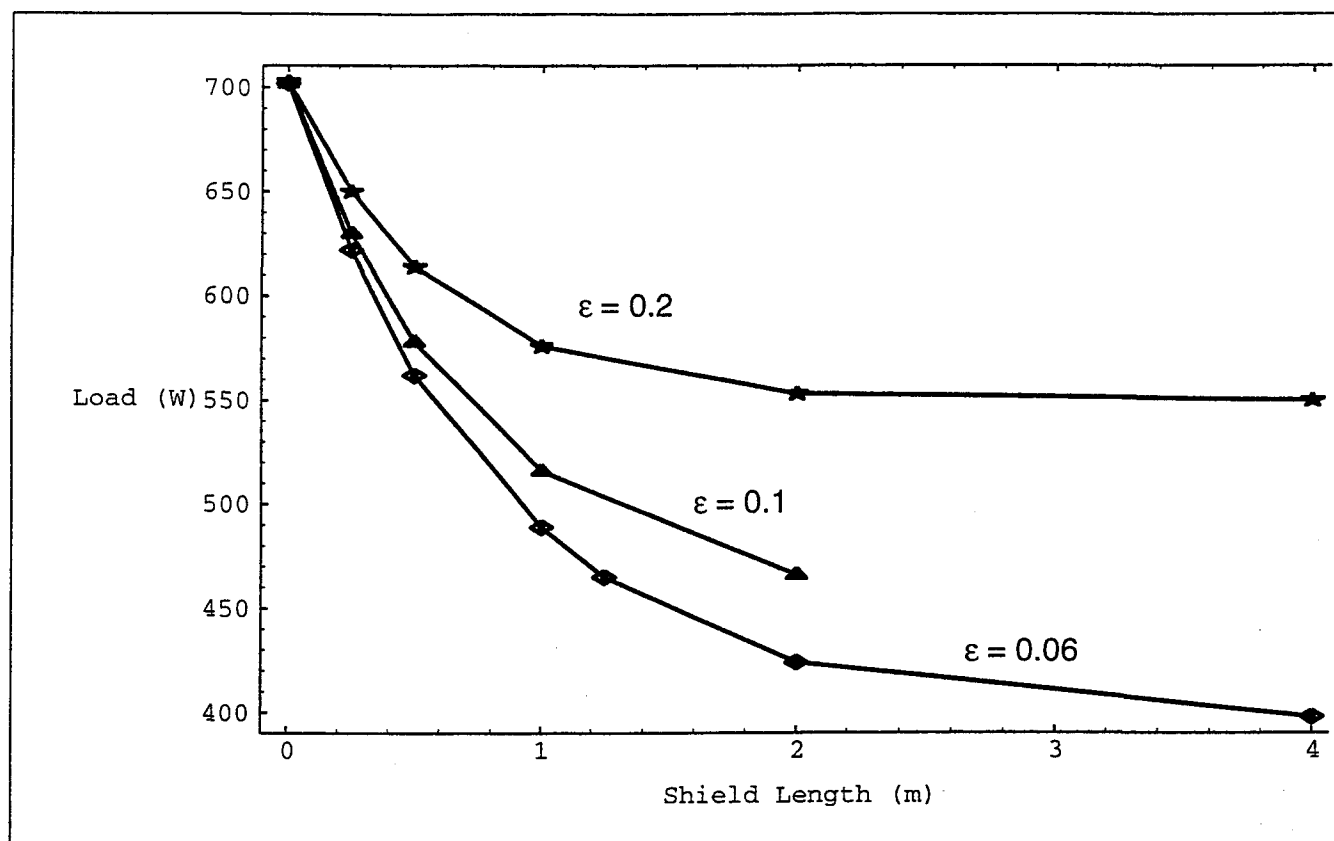


**Figure 3: Short Cryopump Liner (Infrared Shield) Performance
(for liner emissivities of 0.06, 0.10 and 0.20)**



Diffuse Infrared Shield Material

A quick check in the literature and discussions with Dr. Bob Breault (of Breault Research Organization, Inc.) indicates that Flame Sprayed Aluminum (FSA) or gold on FSA can meet the requirements for a low emissivity, diffuse reflector in the infrared. Attached are two references^{1,2}, with BRDF measurements on bare FSA and gold coated FSA. In the second reference, the MIL-STD used in the fabrication of the FSA surface is cited. The directional-hemispherical reflectance at 10.6 microns is approximately 0.85 for bare FSA and 0.95 for gold coated FSA. Both have very flat BRDFs indicating diffuse (Lambertian) behavior for low angles of incidence (as indicated in the attached). As the angle of incidence increases, these materials deviate more from a perfect Lambertian surface with a slight retro-component of reflection and a slight forward scatter (specular) component. However, the deviations from ideal Lambertian behavior are slight (about +/- 15%). The retro-reflection helps in reducing the infrared flux from the beam tube, but increases

1. Oppenheim, U., Turner, M., and Wolfe, W., "BRDF Reference Standards for the Infrared", Infrared Phys. Technol., Vol. 35, No. 7, pp. 873-879, 1994.
2. Brennan, W. (Hughes Electro-Optical & Data Systems Group) to Breault, R., letter with attached data on BRDF of flame sprayed aluminum at 5 deg. angle of incidence and 3 wavelengths (1.06, 3.39 and 10.6 microns), 23 Oct 91.

the coupling of emission from the absorptive side of the laser light baffles placed adjacent to the cold surface.

Considerations Related to the Integration of Laser Light Baffles and Infrared Shields

The minimum diameter of the LN₂ trap based upon considerations of optical shielding of the cold surface from view of the test masses has been addressed in a memorandum by Albert Lazzarini¹. This analysis does not account for the presence of the liners. For the same reasons outlined in this memorandum, the shields (or liners) should not be visible to the test masses, as indicated in Figure 5 (a to-scale drawing).

Stan Whitcomb has pointed out that PSI's proposal to use a diffusive shield in order to reduce the thermal load on the cryo-pump extends the effective length of the cryo-pump considerably resulting in some special considerations in combined IR and optical shielding. The dimensions indicated in the Figure 5 are for the most restrictive baffling situation, i.e. the short cryopumps at the mid- and end-stations. The diameters of the cryopump and its shields result in restricting the maximum length of the liners to about 0.8 m and 1.0 m (for the liner closest to, and farthest from, the test mass respectively) IF no laser light baffles are placed within the infrared liners.

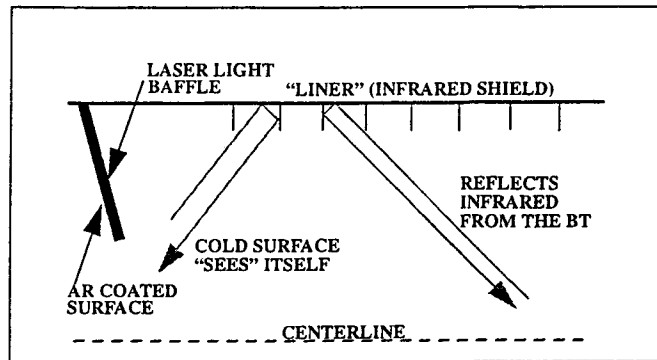
Due to the asymmetric nature of the problem, the two baffles placed between the cold surface and the test mass (Figure 5) serve to absorb laser light on one side and act as a low emissivity infrared radiator on the opposite side. The baffle placed on the side of the cold surface most distant from the test mass (and used to block direct view of the far liner) must be absorptive at the laser wavelength (and therefore absorptive in the infrared as well). Consequently, this baffle will compromise the ideal performance of the liners. However, the view factor from the cold surface to this baffle is not large (as can be seen from the scale drawing, Figure 4). A single baffle to block view of the cold surface and the far liner is impractical (diameter > 1.45 m for a liner of only 0.5 m in length).

An alternative to the use of diffuse liners (suggested by Stan Whitcomb), is to use a retro-reflection surface, as indicated in Figure 4. The cold surface would see itself and the self-emission of the (low emissivity) surface of the liner; The infrared emission of the beam tube would be retro-

1. Lazzarini, A., "Determination of the minimum LN₂ trap inner diameter needed to shield it from direct line of sight from a test mass", LIGO-L950593-01-E, 2 Nov 95.

reflected back down the tube. The performance of this approach is yet to be determined.

Figure 4: Cryopump Liners (Shields)



In either approach for infrared shielding, the laser light baffles adjacent to the cryo pumps would have to be treated differently from the baffles in the beam tube. Stan suggests an broad-band AR coating (from 1 to 10 microns).

DCC:dcc

Attachments:

- 1) Drawing D95~~xxx~~⁰¹⁶²-SK (11/18/95), Cryopump Liner and Baffle Considerations
- 2) Cryopump Radiant Interchange Analysis (derivation and Mathematica Notebook)
- 3) Oppenheim, U., Turner, M., and Wolfe, W., "BRDF Reference Standards for the Infrared", Infrared Phys. Technol., Vol. 35, No. 7, pp. 873-879, 1994.
- 4) Brennan, W. (Hughes Electro-Optical & Data Systems Group) to Breault, R., letter with attached data on BRDF of flame sprayed aluminum at 5 deg. angle of incidence and 3 wavelengths (1.06, 3.39 and 10.6 microns), 23 Oct 91.

Distribution:

W. Althouse	F. Raab	G. Stapfer	J. Worden
M. Coles	G. Sanders	K. Thorne	W. Young
B. Barish	D. Shoemaker	R. Vogt	M. Zucker
D. Jungwirth	A. Sibley	R. Weiss	Chronological File
A. Lazzarini	R. Spero	S. Whitcomb	Document Control Center

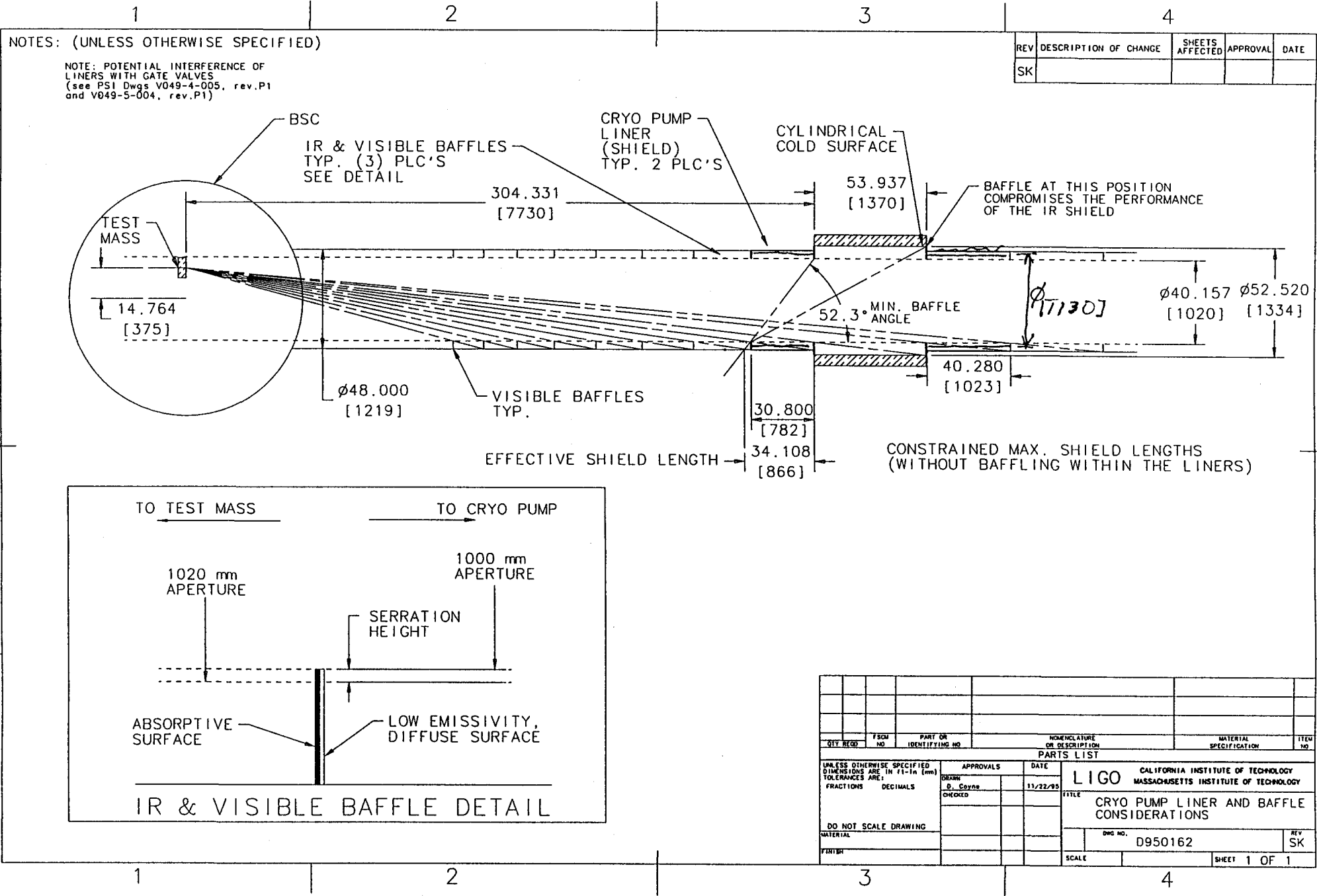
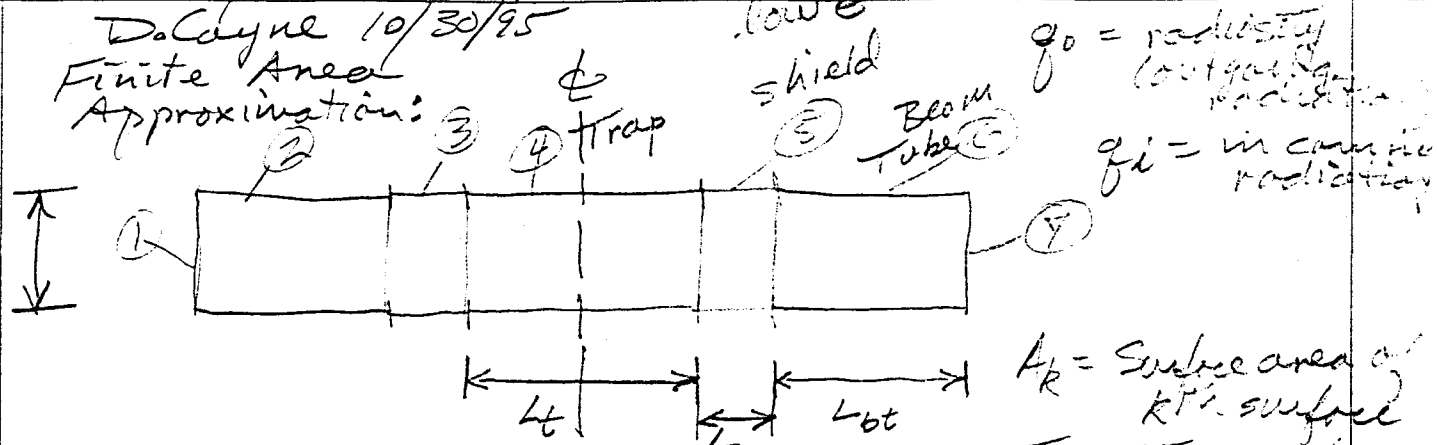


Figure 5.

CRYO PUMP RADIANT INTERCHANGE

DoCayne 10/30/95

Finite Area Approximation:



$q_0 =$ radiosity (outgoing radiation)
 $q_i =$ incoming radiation

$A_k =$ Subarea of k^{th} surface
 $T_k =$ Temperature of k^{th} surface

① $Q_k = \frac{q_k}{f_k} A_k = (q_{0,k} - q_{i,k}) A_k$

② $q_{i,k} = \epsilon_k \sigma T_k^4 + \rho_k q_{i,k} = \epsilon_k \sigma T_k^4 + (1 - \epsilon_k) q_{i,k}$

$$A_k q_{i,k} = A_1 q_{0,1} F_{1-k} + A_2 q_{0,2} F_{2-k} + \dots + A_j q_{0,j} F_{j-k} + \dots + A_k q_{0,k} F_{k-k} + \dots + A_N q_{0,N} F_{N-k}$$

or
 ③ $q_{i,k} = \sum_{j=1}^N F_{k-j} q_{0,j}$ (using the config factor reciprocity relation $A_j F_{j-k} = A_k F_{k-j}$)

from ②:
 $q_{i,k} = \left(\frac{1}{1 - \epsilon_k} \right) (q_{0,k} - \epsilon_k \sigma T_k^4)$
 combining with ①:

$$Q_k = A_k \left[q_{0,k} + \left(\frac{1}{1 - \epsilon_k} \right) (\epsilon_k \sigma T_k^4 - q_{0,k}) \right]$$

④ $Q_k = A_k \left(\frac{\epsilon_k}{1 - \epsilon_k} \right) [\sigma T_k^4 - q_{0,k}]$

combining ① and ③:

⑤ $Q_k = A_k \left(q_{0,k} - \sum_{j=1}^N F_{k-j} q_{0,j} \right)$

13 782 500 SHEETS, FILLED, 5 SQUARE
 42 381 50 SHEETS, CYE EASH, 5 SQUARE
 42 382 100 SHEETS, CYE EASH, 5 SQUARE
 42 383 100 SHEETS, CYE EASH, 5 SQUARE
 42 384 100 SHEETS, CYE EASH, 5 SQUARE
 42 385 100 SHEETS, CYE EASH, 5 SQUARE
 42 386 100 SHEETS, CYE EASH, 5 SQUARE
 42 387 100 SHEETS, CYE EASH, 5 SQUARE
 42 388 100 SHEETS, CYE EASH, 5 SQUARE
 42 389 100 SHEETS, CYE EASH, 5 SQUARE
 42 390 100 SHEETS, CYE EASH, 5 SQUARE
 42 391 100 SHEETS, CYE EASH, 5 SQUARE
 42 392 100 SHEETS, CYE EASH, 5 SQUARE
 42 393 100 SHEETS, CYE EASH, 5 SQUARE
 42 394 100 SHEETS, CYE EASH, 5 SQUARE
 42 395 100 SHEETS, CYE EASH, 5 SQUARE
 42 396 100 SHEETS, CYE EASH, 5 SQUARE
 42 397 100 SHEETS, CYE EASH, 5 SQUARE
 42 398 100 SHEETS, CYE EASH, 5 SQUARE
 42 399 100 SHEETS, CYE EASH, 5 SQUARE
 42 400 100 SHEETS, CYE EASH, 5 SQUARE
 MADE IN U.S.A.
 National Brand

Equations (2) and (3)

$$q_{o,k} - \sum_{j=1}^N F_{k-j} q_{o,j} = \left(\frac{\epsilon_k}{1-\epsilon_k} \right) [\sigma T_k^4 - q_{o,k}]$$

$$q_{o,k} - (1-\epsilon_k) \sum_{j=1}^N F_{k-j} q_{o,j} = \epsilon_k \sigma T_k^4$$

$$\textcircled{6} \quad \sum_{j=1}^N [\delta_{kj} - (1-\epsilon_k) F_{k-j}] q_{o,j} = \epsilon_k \sigma T_k^4$$

$$\textcircled{7} \quad [a] \{q_o\} = \{c\}$$

$$\textcircled{8} \quad \{q_o\} = [a]^{-1} \{c\}$$

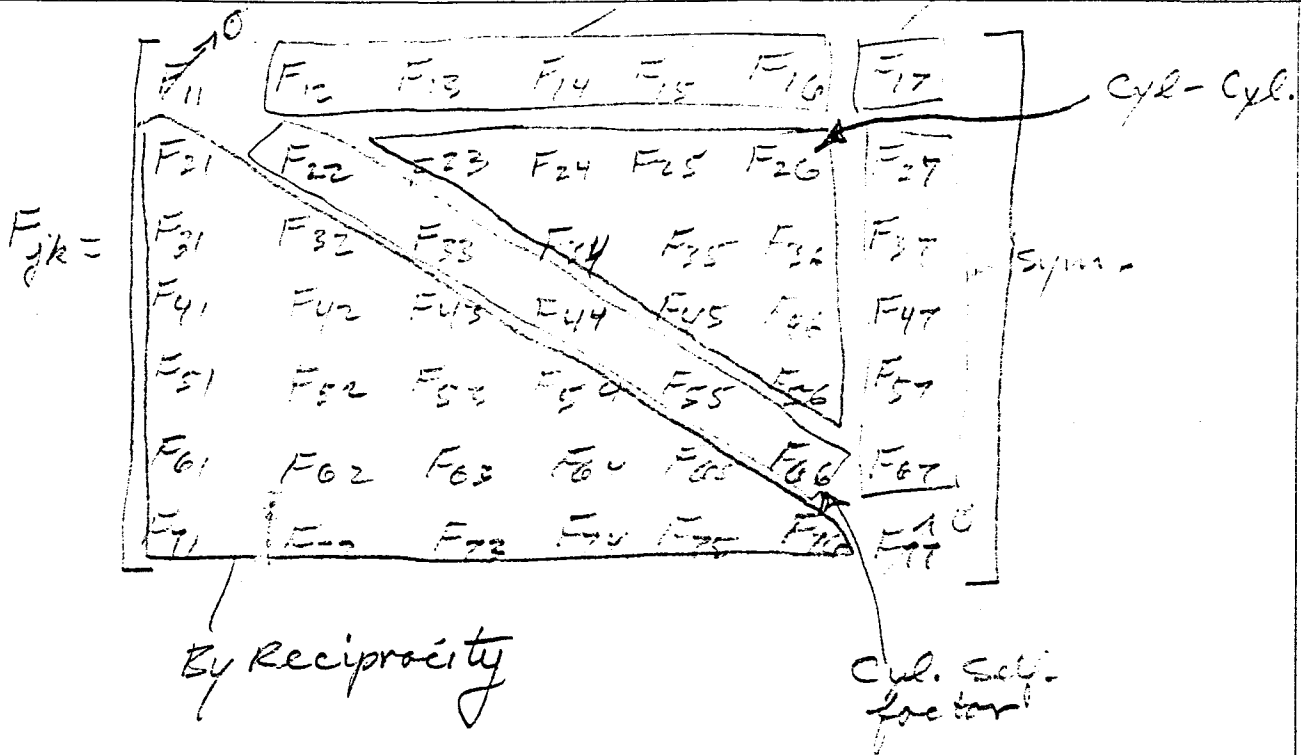
Use

$$\textcircled{5} \quad Q_k = A_k \left(q_{o,k} - \sum_{j=1}^N F_{k-j} q_{o,j} \right)$$

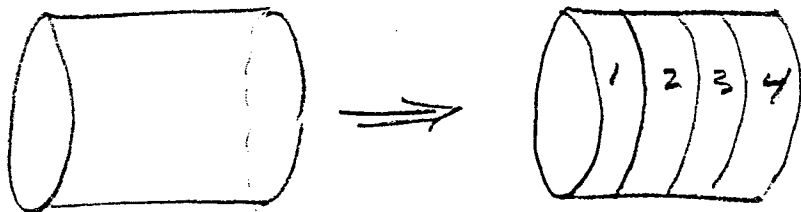
to project out the net heat balance at each surface

disk-cyl.

disk-disk



Discretization of the component geometries is straight forward:



13 702
 42 301
 42 302
 42 303
 42 304
 42 305
 42 306
 42 307
 42 308
 42 309
 42 310
 42 311
 42 312
 42 313
 42 314
 42 315
 42 316
 42 317
 42 318
 42 319
 42 320
 42 321
 42 322
 42 323
 42 324
 42 325
 42 326
 42 327
 42 328
 42 329
 42 330
 42 331
 42 332
 42 333
 42 334
 42 335
 42 336
 42 337
 42 338
 42 339
 42 340
 42 341
 42 342
 42 343
 42 344
 42 345
 42 346
 42 347
 42 348
 42 349
 42 350
 42 351
 42 352
 42 353
 42 354
 42 355
 42 356
 42 357
 42 358
 42 359
 42 360
 42 361
 42 362
 42 363
 42 364
 42 365
 42 366
 42 367
 42 368
 42 369
 42 370
 42 371
 42 372
 42 373
 42 374
 42 375
 42 376
 42 377
 42 378
 42 379
 42 380
 42 381
 42 382
 42 383
 42 384
 42 385
 42 386
 42 387
 42 388
 42 389
 42 390
 42 391
 42 392
 42 393
 42 394
 42 395
 42 396
 42 397
 42 398
 42 399
 42 400
 42 401
 42 402
 42 403
 42 404
 42 405
 42 406
 42 407
 42 408
 42 409
 42 410
 42 411
 42 412
 42 413
 42 414
 42 415
 42 416
 42 417
 42 418
 42 419
 42 420
 42 421
 42 422
 42 423
 42 424
 42 425
 42 426
 42 427
 42 428
 42 429
 42 430
 42 431
 42 432
 42 433
 42 434
 42 435
 42 436
 42 437
 42 438
 42 439
 42 440
 42 441
 42 442
 42 443
 42 444
 42 445
 42 446
 42 447
 42 448
 42 449
 42 450
 42 451
 42 452
 42 453
 42 454
 42 455
 42 456
 42 457
 42 458
 42 459
 42 460
 42 461
 42 462
 42 463
 42 464
 42 465
 42 466
 42 467
 42 468
 42 469
 42 470
 42 471
 42 472
 42 473
 42 474
 42 475
 42 476
 42 477
 42 478
 42 479
 42 480
 42 481
 42 482
 42 483
 42 484
 42 485
 42 486
 42 487
 42 488
 42 489
 42 490
 42 491
 42 492
 42 493
 42 494
 42 495
 42 496
 42 497
 42 498
 42 499
 42 500
 42 501
 42 502
 42 503
 42 504
 42 505
 42 506
 42 507
 42 508
 42 509
 42 510
 42 511
 42 512
 42 513
 42 514
 42 515
 42 516
 42 517
 42 518
 42 519
 42 520
 42 521
 42 522
 42 523
 42 524
 42 525
 42 526
 42 527
 42 528
 42 529
 42 530
 42 531
 42 532
 42 533
 42 534
 42 535
 42 536
 42 537
 42 538
 42 539
 42 540
 42 541
 42 542
 42 543
 42 544
 42 545
 42 546
 42 547
 42 548
 42 549
 42 550
 42 551
 42 552
 42 553
 42 554
 42 555
 42 556
 42 557
 42 558
 42 559
 42 560
 42 561
 42 562
 42 563
 42 564
 42 565
 42 566
 42 567
 42 568
 42 569
 42 570
 42 571
 42 572
 42 573
 42 574
 42 575
 42 576
 42 577
 42 578
 42 579
 42 580
 42 581
 42 582
 42 583
 42 584
 42 585
 42 586
 42 587
 42 588
 42 589
 42 590
 42 591
 42 592
 42 593
 42 594
 42 595
 42 596
 42 597
 42 598
 42 599
 42 600
 42 601
 42 602
 42 603
 42 604
 42 605
 42 606
 42 607
 42 608
 42 609
 42 610
 42 611
 42 612
 42 613
 42 614
 42 615
 42 616
 42 617
 42 618
 42 619
 42 620
 42 621
 42 622
 42 623
 42 624
 42 625
 42 626
 42 627
 42 628
 42 629
 42 630
 42 631
 42 632
 42 633
 42 634
 42 635
 42 636
 42 637
 42 638
 42 639
 42 640
 42 641
 42 642
 42 643
 42 644
 42 645
 42 646
 42 647
 42 648
 42 649
 42 650
 42 651
 42 652
 42 653
 42 654
 42 655
 42 656
 42 657
 42 658
 42 659
 42 660
 42 661
 42 662
 42 663
 42 664
 42 665
 42 666
 42 667
 42 668
 42 669
 42 670
 42 671
 42 672
 42 673
 42 674
 42 675
 42 676
 42 677
 42 678
 42 679
 42 680
 42 681
 42 682
 42 683
 42 684
 42 685
 42 686
 42 687
 42 688
 42 689
 42 690
 42 691
 42 692
 42 693
 42 694
 42 695
 42 696
 42 697
 42 698
 42 699
 42 700
 42 701
 42 702
 42 703
 42 704
 42 705
 42 706
 42 707
 42 708
 42 709
 42 710
 42 711
 42 712
 42 713
 42 714
 42 715
 42 716
 42 717
 42 718
 42 719
 42 720
 42 721
 42 722
 42 723
 42 724
 42 725
 42 726
 42 727
 42 728
 42 729
 42 730
 42 731
 42 732
 42 733
 42 734
 42 735
 42 736
 42 737
 42 738
 42 739
 42 740
 42 741
 42 742
 42 743
 42 744
 42 745
 42 746
 42 747
 42 748
 42 749
 42 750
 42 751
 42 752
 42 753
 42 754
 42 755
 42 756
 42 757
 42 758
 42 759
 42 760
 42 761
 42 762
 42 763
 42 764
 42 765
 42 766
 42 767
 42 768
 42 769
 42 770
 42 771
 42 772
 42 773
 42 774
 42 775
 42 776
 42 777
 42 778
 42 779
 42 780
 42 781
 42 782
 42 783
 42 784
 42 785
 42 786
 42 787
 42 788
 42 789
 42 790
 42 791
 42 792
 42 793
 42 794
 42 795
 42 796
 42 797
 42 798
 42 799
 42 800
 42 801
 42 802
 42 803
 42 804
 42 805
 42 806
 42 807
 42 808
 42 809
 42 810
 42 811
 42 812
 42 813
 42 814
 42 815
 42 816
 42 817
 42 818
 42 819
 42 820
 42 821
 42 822
 42 823
 42 824
 42 825
 42 826
 42 827
 42 828
 42 829
 42 830
 42 831
 42 832
 42 833
 42 834
 42 835
 42 836
 42 837
 42 838
 42 839
 42 840
 42 841
 42 842
 42 843
 42 844
 42 845
 42 846
 42 847
 42 848
 42 849
 42 850
 42 851
 42 852
 42 853
 42 854
 42 855
 42 856
 42 857
 42 858
 42 859
 42 860
 42 861
 42 862
 42 863
 42 864
 42 865
 42 866
 42 867
 42 868
 42 869
 42 870
 42 871
 42 872
 42 873
 42 874
 42 875
 42 876
 42 877
 42 878
 42 879
 42 880
 42 881
 42 882
 42 883
 42 884
 42 885
 42 886
 42 887
 42 888
 42 889
 42 890
 42 891
 42 892
 42 893
 42 894
 42 895
 42 896
 42 897
 42 898
 42 899
 42 900
 42 901
 42 902
 42 903
 42 904
 42 905
 42 906
 42 907
 42 908
 42 909
 42 910
 42 911
 42 912
 42 913
 42 914
 42 915
 42 916
 42 917
 42 918
 42 919
 42 920
 42 921
 42 922
 42 923
 42 924
 42 925
 42 926
 42 927
 42 928
 42 929
 42 930
 42 931
 42 932
 42 933
 42 934
 42 935
 42 936
 42 937
 42 938
 42 939
 42 940
 42 941
 42 942
 42 943
 42 944
 42 945
 42 946
 42 947
 42 948
 42 949
 42 950
 42 951
 42 952
 42 953
 42 954
 42 955
 42 956
 42 957
 42 958
 42 959
 42 960
 42 961
 42 962
 42 963
 42 964
 42 965
 42 966
 42 967
 42 968
 42 969
 42 970
 42 971
 42 972
 42 973
 42 974
 42 975
 42 976
 42 977
 42 978
 42 979
 42 980
 42 981
 42 982
 42 983
 42 984
 42 985
 42 986
 42 987
 42 988
 42 989
 42 990
 42 991
 42 992
 42 993
 42 994
 42 995
 42 996
 42 997
 42 998
 42 999
 42 1000



CRYO PUMP RADIANT INTERCHANGE

■ Cryo Pump Properties

■ Component Dimensions

In[2790]:=

```
Dia = 1.22;      (* m *)  
Ltrap = 3.7;    (*large cryo-pump, m *)  
Lshield = 1.5;  (* m *)  
Lbt = 20;      (* m *)
```

In[2794]:=

```
radius = Dia/2;  
L = Ltrap + 2 (Lshield + Lbt);    (* overall length, m *)
```

■ Component Emissivities

In[2796]:=

```
eend = 0.9;      (* emissivity of the bt ends *)  
ebt = 0.5;      (* emissivity of the beam tube *)  
eshield = 0.06; (* emissivity of the shields *)  
etrap = 1.0;    (* emissivity of the cold trap *)
```

■ Component Temperatures (K)

In[2800]:=

```
Tend = 295;  
Tbt = 295;  
Tshield = 295;  
Ttrap = 80;
```

■ Cryo Pump Model Parameters

■ Segmentation

In[2804]:=

```
ntrap = 10;      (* number of segments for the cold trap surface *)
nshield = 10;   (* number of segments for each shield surface *)
nbt = 20;      (* number of segments for each beam tube surface *)
n = 2 + 2 (nbt + nshield) + ntrap
```

Out[2807]=

72

■ Segmented Surface Area, Position, Length, Emissivity & Temperature

In[2808]:=

```
A = Table[0, {n}];
emiss = A;
T = A;
x = A;
s = A;
A[[1]] = Pi Dia^2/4;
A[[n]] = A[[1]];
emiss[[1]] = eend;
emiss[[n]] = emiss[[1]];
T[[1]] = Tend;
T[[n]] = T[[1]];
x[[1]] = 0;
x[[n]] = L;
s[[1]] = 0;
s[[n]] = 0;
```

In[2823]:=

```

As = Pi Dia Lbt/nbt;
es = ebt;
Ts = Tbt;
ss = Lbt/nbt;
Do [
  A[[i]] = As;
  emiss[[i]] = es;
  T[[i]] = Ts;
  s[[i]] = ss;
  x[[i]] = x[[i-1]] + s[[i-1]];
  A[[i+nbt+ntrap+2 nshield]] = As;
  emiss[[i+nbt+ntrap+2 nshield]] = es;
  T[[i+nbt+ntrap+2 nshield]] = Ts;
  s[[i+nbt+ntrap+2 nshield]] = ss;
  x[[i+nbt+ntrap+2 nshield]] = x[[i]] + Lbt + Ltrap + 2 Lshield,
  {i,2,nbt+1}
];
As = Pi Dia Lshield/nshield;
es = eshield;
Ts = Tshield;
ss = Lshield/nshield;
Do [
  A[[i]] = As;
  emiss[[i]] = es;
  T[[i]] = Ts;
  s[[i]] = ss;
  x[[i]] = x[[i-1]] + s[[i-1]];
  A[[i+nshield+ntrap]] = As;
  emiss[[i+nshield+ntrap]] = es;
  T[[i+nshield+ntrap]] = Ts;
  s[[i+nshield+ntrap]] = ss;
  x[[i+nshield+ntrap]] = x[[i]] + Lshield + Ltrap,
  {i,nbt+2,nbt+nshield+1}
];
As = Pi Dia Ltrap/ntrap;
es = etrap;
Ts = Ttrap;
ss = Ltrap/ntrap;
Do [
  A[[i]] = As;
  emiss[[i]] = es;
  T[[i]] = Ts;
  s[[i]] = ss;
  x[[i]] = x[[i-1]] + s[[i-1]],
  {i,nbt+nshield+2,nbt+nshield+ntrap+1}
];

```

■ View Factors

```
In[2838]:=
  F = Table[0, {n}, {n}];
```

■ Disk-Disk View Factors

N.B.: Concentric, r1 and r2 are radii, h = distance between disks

```
In[2839]:=
  Fdd[r1_, r2_, h_] := If[h == 0, 1,
  With[{X = 1 + (1 + (r2/h)^2) / (r1/h)^2}, 1/2 (X - Sqrt[X^2 - 4
  (r2/r1)^2])]];

```

Left End Disk(1) - Right End Disk(n):

```
In[2840]:=
  F[[1, n]] = Fdd[Dia/2, Dia/2, L];
```

■ Disk-Interior Cylinder View Factors

N.B.: Concentric, r1 = disk radius, r2 = cylinder radius, r1 <= r2, h1 = distance from disk to near end of cylinder, h2 = distance from disk to far end of cylinder

```
In[2841]:=
  Fdc[r1_, r2_, h1_, h2_] := Fdd[r1, r2, h1] - Fdd[r1, r2, h2];
```

Left End Disk(1) - Cylindrical Segments (2->n-1)
and by symmetry, Cylindrical Segments (2->n-1) - Right End Disk(n):

```
In[2842]:=
  Do [
    F[[1, i]] = Fdc[radius, radius, x[[i]], x[[i]] + s[[i]]];
    j = n - i + 1;
    F[[j, n]] = F[[1, i]] A[[n]] / A[[j]],
    {i, 2, n - 1}
  ];
```

■ Interior Cylinder Self-View Factors

N.B.: r = radius, l = cylinder length

```
In[2843]:=
  Fcself[r_, l_] := 1 - (r/l) Fdc[r, r, 0, l];
```

Cylindrical Segments (i) - Cylindrical Segments (i), for $i=\{2,n-1\}$:

```
In[2844]:=
Do [
  F[[i,i]] = Fcself[radius,s[[i]],
    {i,2,n-1}
];
```

■ Interior Equal-Diameter Concentric Cylinder View Factors

N.B.: r = radius, l_1 = cylinder 1 length, l_2 = cylinder 2 length, h = separation distance

```
In[2845]:=
Fceq[r_,l1_,l2_,h_] := (Fdc[r,r,h,l1+h] - Fdc[r,r,l2+h,l2+l1+h]) (r/(2 l
```

Cylindrical Segments (i) - Cylindrical Segments (j), for $i,j=\{2,n-1\}$:

```
In[2846]:=
Ftemp=Table[0,{n},{n}];

In[2847]:=
Do [
  Do [
    F[[i,j]] = Fceq[radius,s[[i]],s[[j]],x[[j]]-x[[i]]-s[[i]];
    Ftemp[[i,j]] = F[[i,j]],
    {j,i+1,n-1}
  ],
  {i,2,n-2}
];
```

■ Reciprocity

```
In[2848]:=
Do [
  Do [
    F[[i,j]] = F[[j,i]] A[[j]]/A[[i]],
    {j,1,i-1},
    {i,2,n}];
Do [
  Print[Sum[F[[i,j]],{j,1,n}],
    {i,1,n}];
```


■ Radiant Exchange Solution

```

In[2849]:=
  one = Table[1, {n}];
  a = IdentityMatrix[n] - Dot[DiagonalMatrix[(one - emiss)], F];

In[2851]:=
  stefanBoltzmann = 5.6696 10^-8; (* W/m^2/K^4 *)
  b = stefanBoltzmann emiss T^4;

In[2853]:=
  q0 = Inverse[a].b;

In[2854]:=
  q = q0 - F.q0 //N;

In[2855]:=
  Q = Dot[DiagonalMatrix[A], (q0 - F.q0)] //N;

In[2856]:=
  Qends = Q[[1]] + Q[[n]]

Out[2856]=
  0.302877

In[2857]:=
  Qbts = Sum[Q[[i]], {i, 2, nbt+1}] + Sum[Q[[i]], {i, nbt+ntrap+2,
  nshield+2, n-1}]

Out[2857]=
  363.647

In[2858]:=
  Qshields = Sum[Q[[i]], {i, nbt+2, nbt+nshield+1}]
  + Sum[Q[[i]], {i, nbt+nshield+ntrap+2, nbt+ntrap+2, nshield+1}]

Out[2858]=
  138.878

In[2859]:=
  Qtrap = Sum[Q[[i]], {i, nbt+nshield+2, nbt+nshield+ntrap+1}]

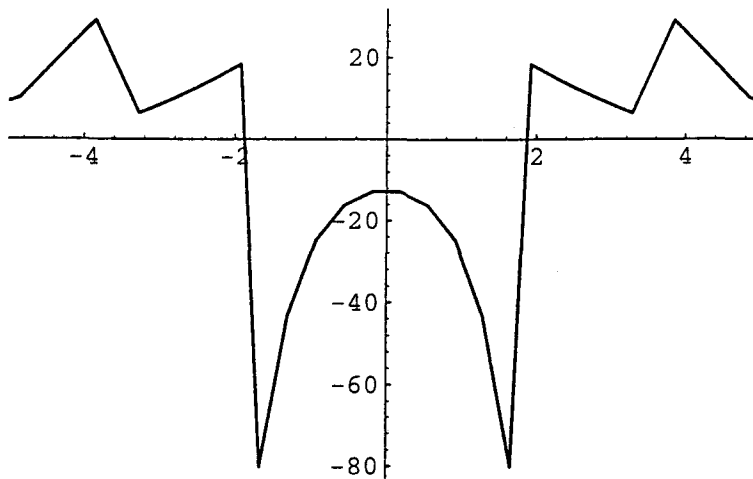
Out[2859]=
  -502.828

In[2860]:=
  xmid = x + s/2 - L/2;

```

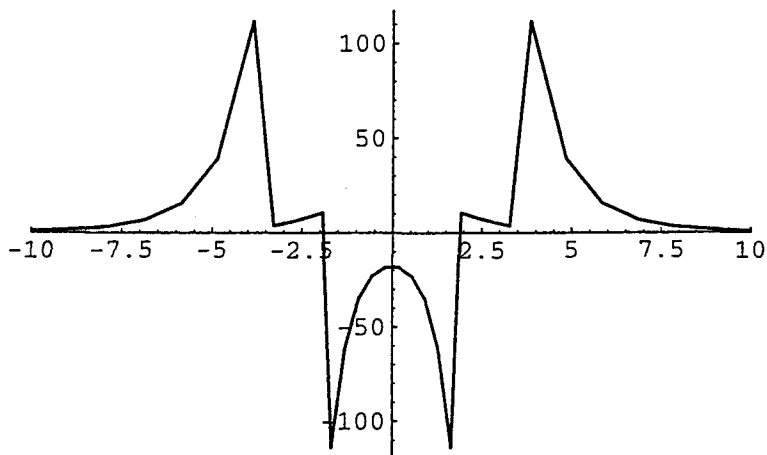
In[2861]:=

```
ListPlot[Transpose[Partition[Join[xmid,q],n]],PlotJoined->True,PlotRange->{{-5,5},All}];
```



In[2862]:=

```
ListPlot[Transpose[Partition[Join[xmid,Q],n]],PlotJoined->True,PlotRange->{{-10,10},All}];
```



■ Tabulated Results

■ Long Cryo-Pump

1.2 m diameter
 3.7 m long cold trap
 nominally 1.52 m long shields (liners)
 trap emissivity = 1.0 (ice)
 shield emissivity = 0.06 (diffuse)
 beam tube model length = 20 m

shield emissivity = 0.06

nbt = 20

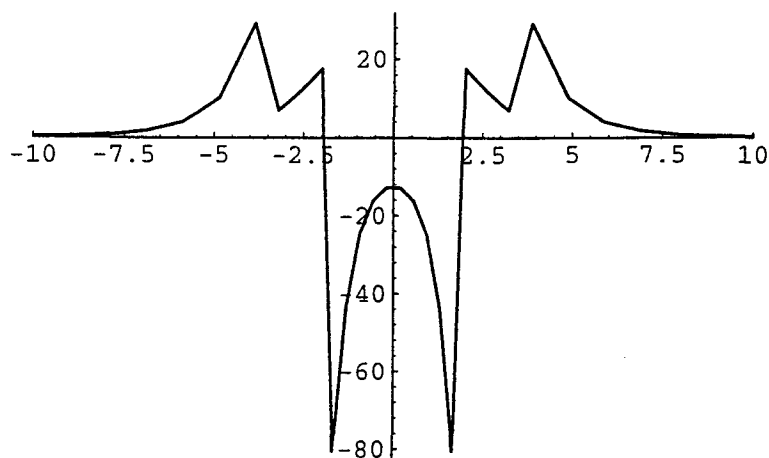
nshield = 5

ntrap = 10

n = 62

Qtrap = 504 W

q (W/m²) vs Xmid (m) :



shield emissivity = 0.5

nbt = 20

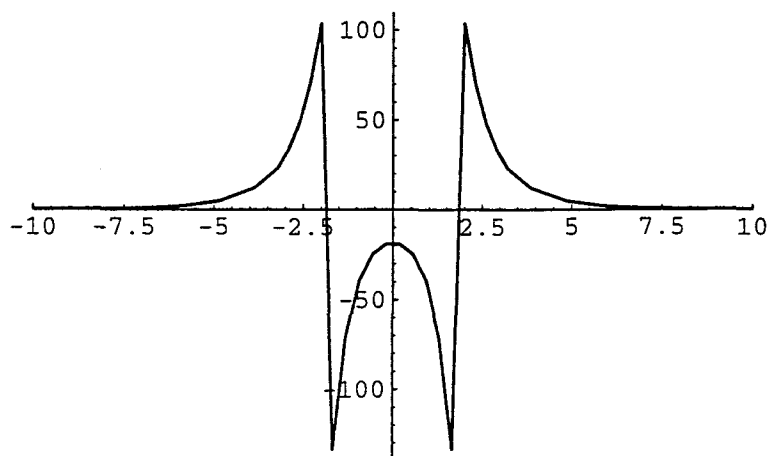
nshield = 5

ntrap = 10

n = 62

Qtrap = 817 W (823 W when Lshield == 3 m)

q (W/m²) vs Xmid (m) :



In[2863]:=

Needs ["Graphics`MultipleListPlot`"]

Used nshield = 10, for a no-shield resulting Q = 815 W in the following sensitivity calculations to shield emissivity and length:

```
In[2864]:=
```

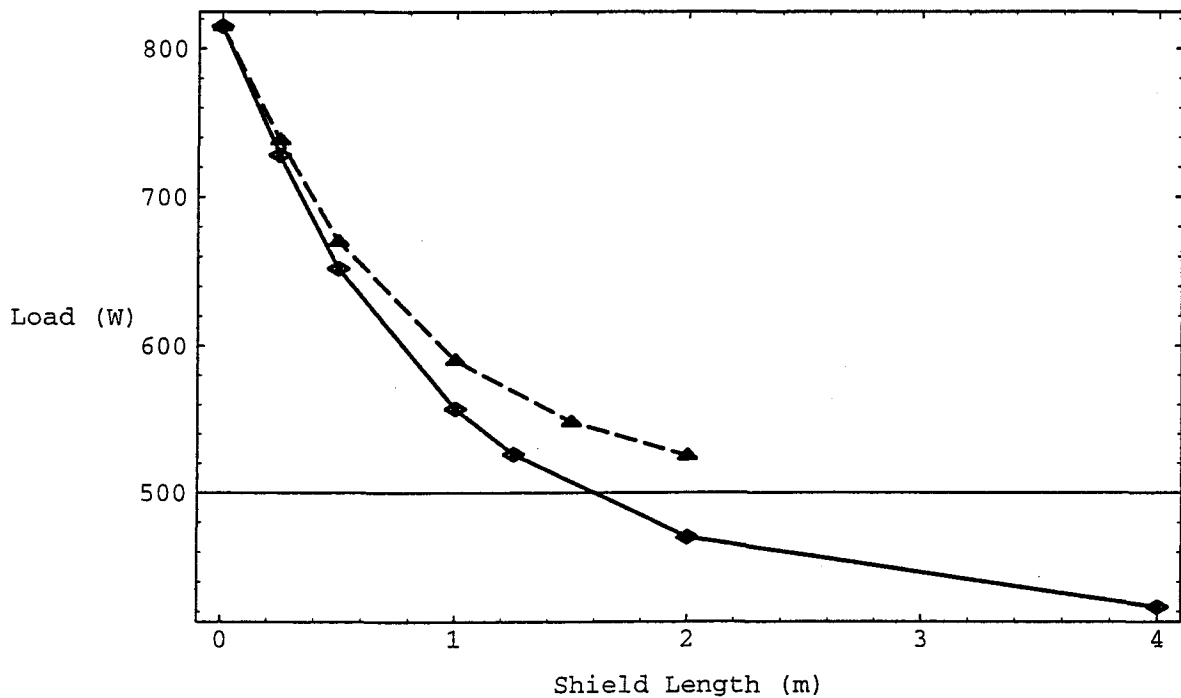
```
emissShield = {0.06, 0.10};
```

```
In[2865]:=
```

```
Qlong = {{{0,815}, {0.25,728}, {0.5,652}, {1.0,557},
{1.25,526}, {2,470}, {4,423}},
{{0,815},{0.25,738}, {0.5,670}, {1,590}, {1.5,548}, {2,525}}};
```

```
In[2866]:=
```

```
MultipleListPlot[Qlong[[1]],Qlong[[2]],PlotJoined-
>True,PlotRange->All,LineStyles-
>{{},{Dashing[{0.02,0.01]}},{Dashing[{0.03,0.01,0.01,0.01]}]},
Frame->True, RotateLabel->False, FrameLabel->{"Shield Length
(m)", "Load (W)"}];
```



Heat load (W) on the inner surface of the cryo-pump (cold trap) for the "long" (3.7 m) cryo-pump, as a function of shield length (m) parameterized by emissivity (0.06, 0.10 and 0.20).

■ Short Cryo-Pump

1.2 m diameter
 1.2 m long cold trap
 1 m long shields (liners)
 trap emissivity = 1.0 (ice)
 shield emissivity = 0.06 (diffuse)
 beam tube model length = 10 m

shield emissivity = 0.06

nbt = 20

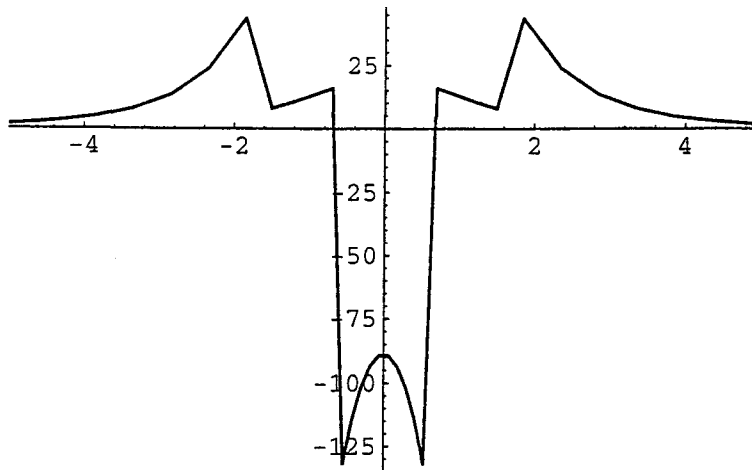
nshield = 5

ntrap = 10

n = 62

Qtrap = 489 W

q (W/m²) vs Xmid (m) :



shield emissivity = 0.5

nbt = 20

nshield = 5

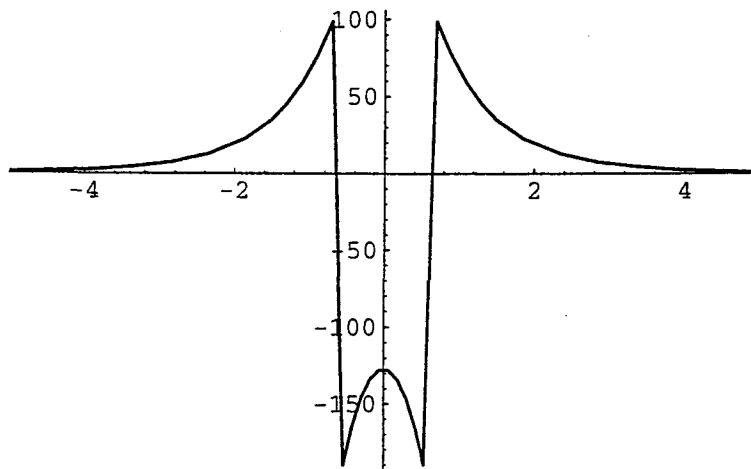
ntrap = 10

n = 62

Qtrap = 702 W (when Lshield == 1 m)

Qtrap = 708 W (when Lshield == 3 m)

q (W/m²) vs Xmid (m) :



Note: Used 10 segments for the shield when the emissivity of the shield was set to 0.2

In[2867]:=

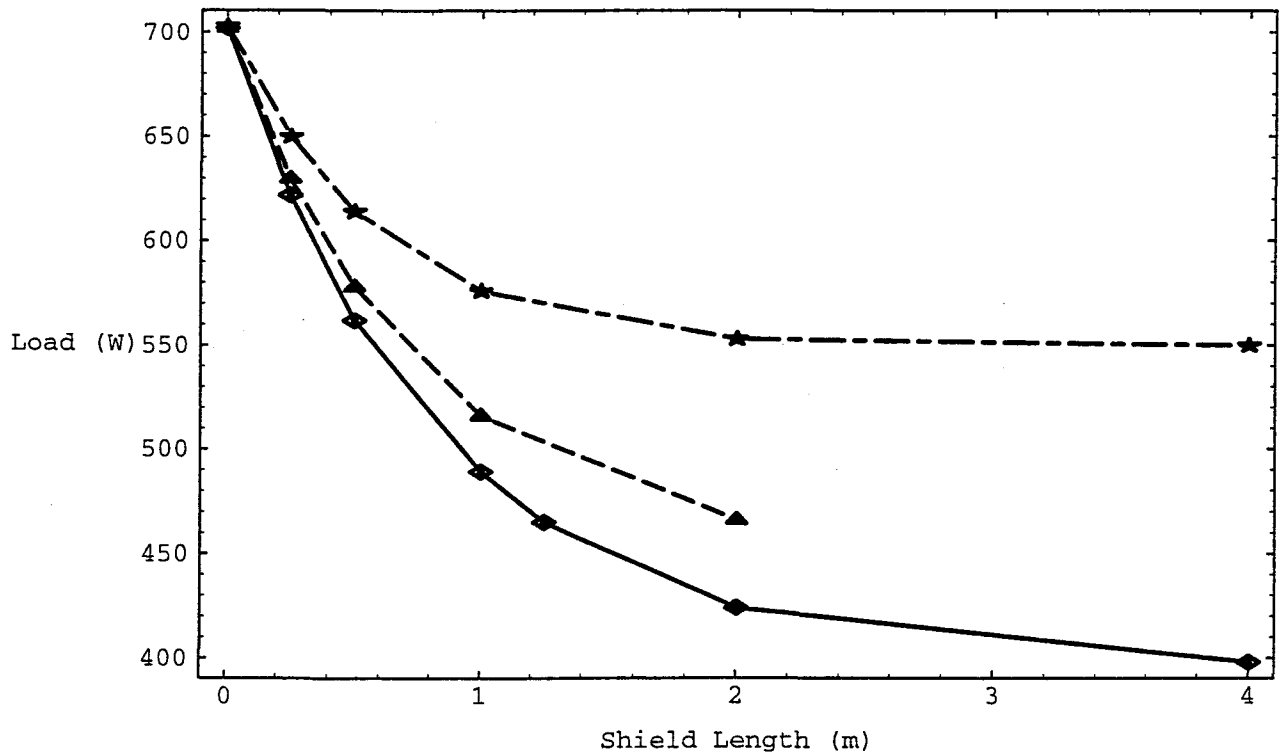
```
emissShield = {0.06, 0.10, 0.20};
```

In[2868]:=

```
Qshort = {{{0,702}, {0.25,622}, {0.5,562}, {1.0,489},
{1.25,465}, {2,424}, {4,398}},
{{0,702},{0.25,630}, {0.5,578}, {1,516}, {2,466}},
{{0,703}, {0.25,650}, {0.5,614}, {1,576}, {2,553}, {4,550}}};
```

In[2869]:=

```
MultipleListPlot[Qshort[[1]],Qshort[[2]],Qshort[[3]],PlotJoined-
->True,PlotRange->All,LineStyle-
>{{}, {Dashing[{0.02,0.01}]}, {Dashing[{0.03,0.01,0.01,0.01}]}}},
Frame->True, RotateLabel->False, FrameLabel->{"Shield Length
(m)", "Load (W)"}];
```



Heat load (W) on the inner surface of the cryo-pump (cold trap) for the "short" (1.2 m) cryo-pump, as a function of shield length (m) parameterized by emissivity (0.06, 0.10 and 0.20).

D. Coyne



Pergamon

1350-4495(94)00034-4

Infrared Phys. Technol. Vol. 35, No. 7, pp. 873-879, 1994
Copyright © 1994 Elsevier Science Ltd
Printed in Great Britain. All rights reserved
1350-4495/94 \$7.00 + 0.00

BRDF REFERENCE STANDARDS FOR THE INFRARED

URI P. OPPENHEIM,[†] MARY G. TURNER and W. L. WOLFE

Optical Sciences Center, University of Arizona, Tucson, AZ 85721, U.S.A.

(Received 24 April 1994)

Abstract—A comparison between various recommended reference standards of diffuse reflectance in the IR is presented. It is shown that at a wavelength of 10.6 μm sulfur is the most Lambertian of the tested samples, although its powdery consistence makes it less suitable for use as a standard. Flame sprayed aluminum, with or without gold coating, also approaches a Lambertian surface and is suitable for use as a standard for BRDF measurements at 10.6 μm . Results for the BRDF of sulfur, gold-coated sandpaper, a commercial diffuse gold surface (by Labsphere) and flame sprayed aluminum are presented.

INTRODUCTION

Round Robin studies of the Bidirectional Reflectance Distribution Function (BRDF) of surfaces in the infrared^(1,2) have proved the need for better reference standards and improved measurement techniques in this region of the spectrum. The latest report⁽³⁾ shows differences in BRDF values of up to 50% between laboratories. There is a need for highly diffuse surfaces which are also highly reflecting in the IR and at the same time are sturdy and reproducible.

The present study is a comparison between several candidates for diffuse standards made with the AZSCAT [Arizona Scatterometer⁽⁴⁾] situated in the Optical Sciences Center of the University of Arizona. The source of radiation was a chopped cw CO₂ laser, polarized in the vertical direction which was always normal to the plane of incidence of the sample. The samples available for this study were sulfur, gold-coated sandpaper, a commercial diffuse gold surface and flame sprayed aluminum (bare and gold-coated). Angles of incidence were chosen at 10, 30, 45 and 60°. BRDF measurements for all these samples are presented.

Although no specular reflectance peak was observed for these samples (except the commercial sample), a distinct "retro" effect was observed, showing a hump in the BRDF curve at a backscatter angle equal to the angle of incidence. Slight departures from Lambertian behavior were observed at angles of incidence of 45 and 60°, although the surfaces were still highly diffuse.

MEASUREMENTS AND RESULTS

The following samples were available for the present study:

1. Flowers of sulfur, also known as sublimed sulfur powder. The sample was prepared by mixing the powder with acetone and compressing it in a tray, according to the "sulfur flooded" method described by Haner and Menzies.⁽⁵⁾ The sample had a diameter of 5 cm.
2. Gold-coated sandpaper. This surface was available from previous studies at the Optical Sciences Center and was described by Stuhlinger *et al.*⁽⁶⁾ A sample of 600 grit gold-coated sandpaper of 5 cm dia. was used.
3. A "certified reflectance standard" obtained from Labsphere (North Sutton, NH) of 5 cm dia., No. IRS-94-020. This consisted of a coarse sandblasted, gold electroplated surface.

[†]On ׁׂ׃ׄ (sabbatical leave) from the Technion-Israel Institute of Technology, Haifa, Israel.

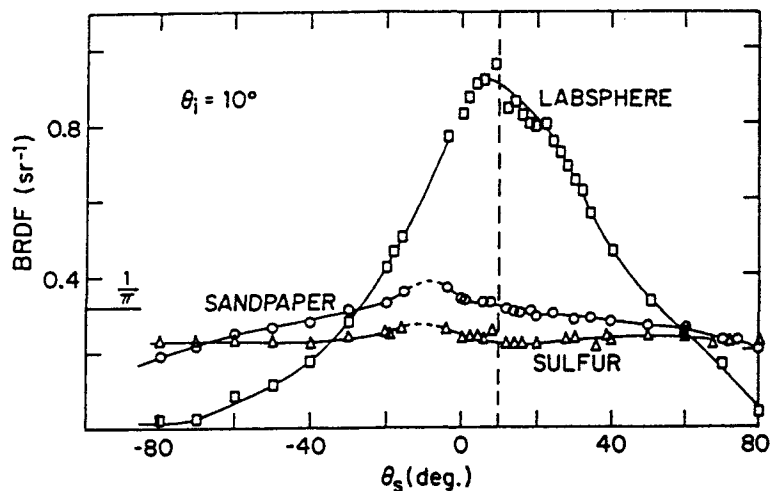


Fig. 1. BRDF of three samples at $10.6 \mu\text{m}$ for an angle of incidence of 10° .

4. Flame sprayed aluminum, made by flame spraying a flat aluminum surface, 5×5 cm in size, with an appearance that was much coarser than the Labsphere sample. Visual inspection of this surface showed many shiny dots which moved along the surface as the viewing angle was changed.
5. Gold-coated flame sprayed aluminum. This was obtained by having a sample of flame sprayed aluminum electroplated with pure gold. The plating was done by a process called "laser gold" by Epner Technology, Inc. (25 Division Place, Brooklyn, NY 11222).

All measurements were made with the AZSCAT instrument, which is fully automatic and is

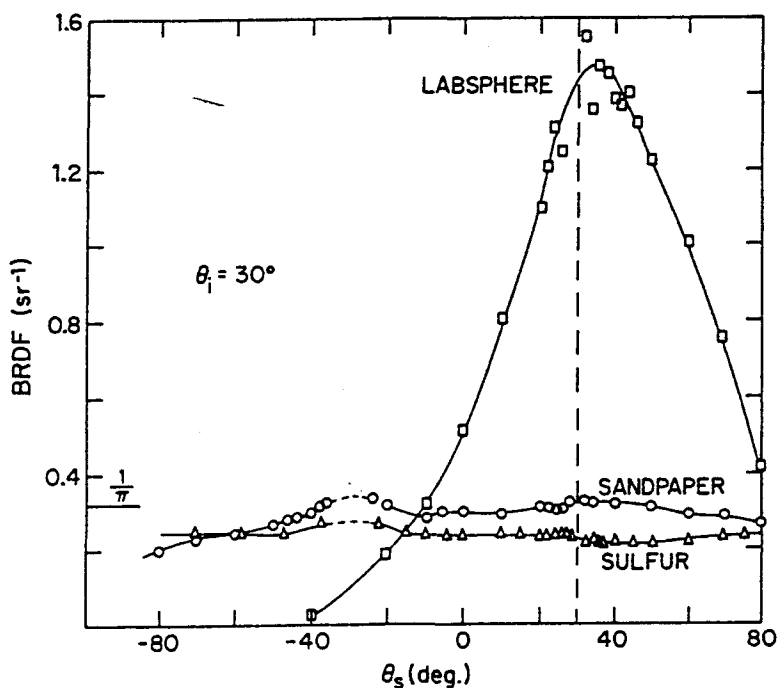


Fig. 2. BRDF of three samples at $10.6 \mu\text{m}$ for an angle of incidence of 30° .

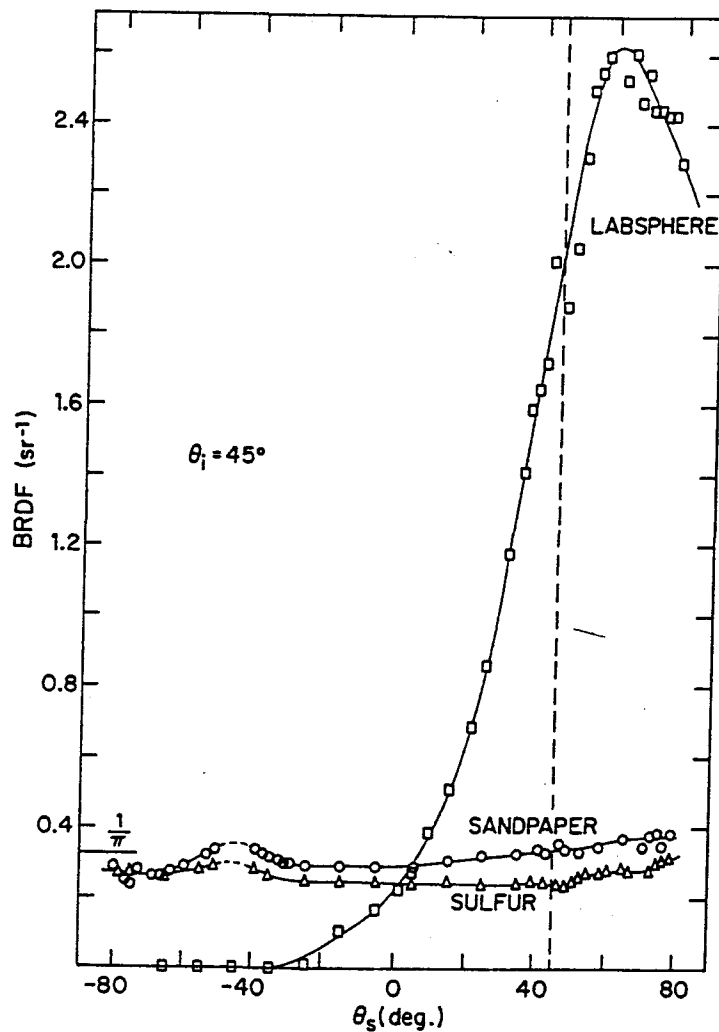


Fig. 3. BRDF of three samples at 10.6 μm for an angle of incidence of 45°.

based on the single reference method.⁽⁴⁾ The BRDF is calculated using the relation

$$\text{BRDF} = \frac{\rho}{\pi} \frac{V_i}{V_o \cos \theta_s}$$

where ρ is the directional-hemispherical reflectance, V_i is the output of the detector for the sample under study, V_o is the detector output for the reference sample and θ_s is the scattering angle with respect to the normal to the surface. Before a run of BRDF measurements of a certain sample was started, the gold-coated sandpaper was used as a reference by placing it in the beam at an angle of incidence of 10° and a scattering angle of 5°. The detector output in this position was taken as V_o in the runs that followed. It was assumed that the hemispherical reflectance of the gold sandpaper was 0.97 in this position, and this value was used in the above expression for the BRDF. Once this value was established the BRDF for any given sample and any pair of angles could be measured by the instrument.

All measurements were made with the incident and scattered beams in the plane of incidence of the sample, so that the azimuthal scattering angle was zero at all times. The instrument was capable of spinning the sample around an axis normal to the sample plane and this was done in all measurements, in order to eliminate speckle effects. The output of the laser was polarized in the vertical direction, but since the detector was not sensitive to the plane of polarization these effects were not taken into account in the present study.

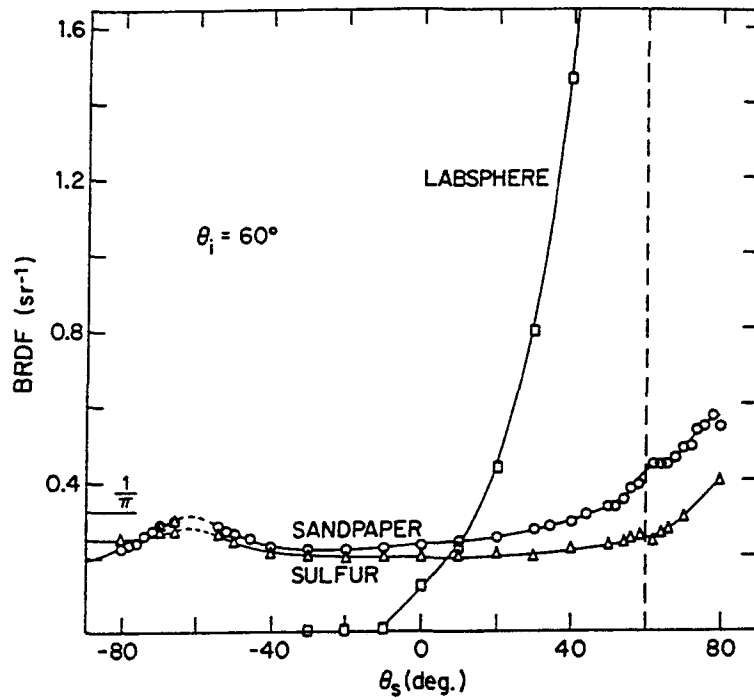


Fig. 4. BRDF of three samples at $10.6 \mu\text{m}$ for an angle of incidence of 60° .

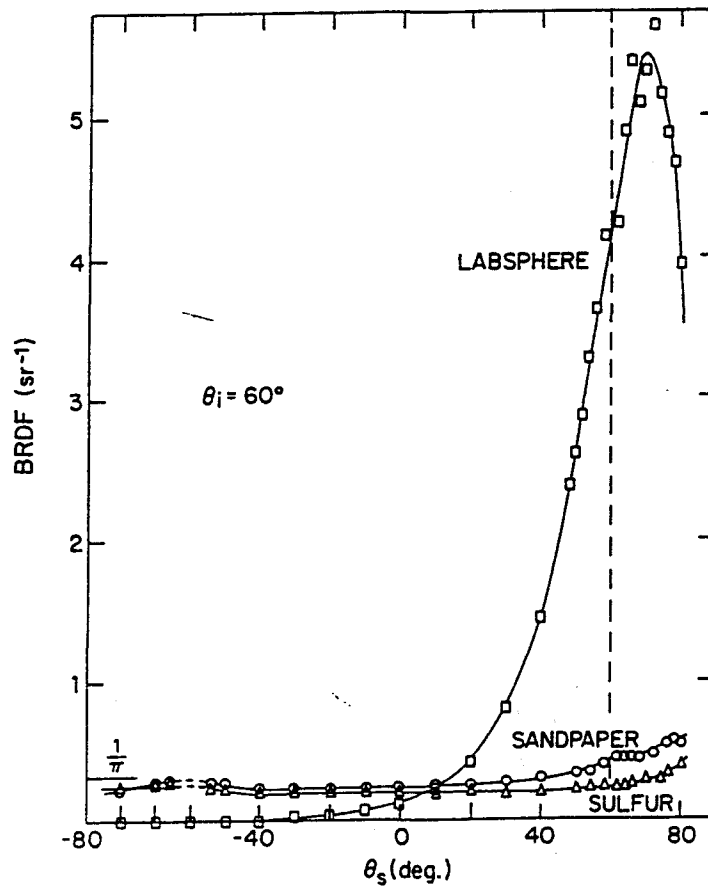


Fig. 5. BRDF of three samples at $10.6 \mu\text{m}$ for an angle of incidence of 60° (note change of scale of ordinate axis).

Figures 1-5 show the results of BRDF for the samples of sulfur, gold-coated sandpaper and Labsphere gold. In each figure the angle of incidence is constant and the scattering angle is shown on the abscissa, with positive angles signifying forward scattering and negative angles indicating backscattering. The angle of incidence is noted as θ_i in each figure. Several results are evident:

1. While sulfur and sandpaper are fairly constant as a function of θ_s , showing a fairly Lambertian behavior, the Labsphere sample has a distinct peak around the specular reflection angle. A closer look at this peak shows that at higher angles of incidence (45 and 60°) the peaks occur at scattering angles which are higher than the specular angle. This is the well-known off-specular effect, which was described and calculated by Torrance and Sparrow.⁽⁷⁾
2. A small peak is observed at the "retro" angle which is equal to the negative of the specular angle and is due to radiation which is backscattered in the direction of the incident beam. This effect was studied recently by Gu *et al.*⁽⁸⁾

Subsequent to these measurements several samples of flame sprayed aluminum (FSA) were obtained, both gold-coated and bare. The results of BRDF measurements for these samples are shown in Fig. 6, where the two types of FSA are compared at angles of incidence of 10 and 45°. It is seen that the bare FSA has a BRDF which is approx. 85% of the BRDF of its gold-coated counterpart. Since the gold-coated FSA was fairly Lambertian and highly reflective its BRDF was more fully measured at angles of incidence of 10, 30, 45 and 60° (see Fig. 7). It is seen that as the angle of incidence increases, this surface deviates from Lambertian behavior. While there is never a specular peak, the BRDF curves at $\theta_i = 45$ and 60° rise at the higher scattering angles (above $\theta_s = 50^\circ$), showing "glint". This is apparently unavoidable in these metal surfaces. At the same time there is also a pronounced "retro" hump in these curves.

A comparison between the results for sandpaper in Figs 1-5 with those on gold-coated FSA in Fig. 7 showed that at small angles of incidence the two surfaces gave BRDF's which were equal to within $\pm 5\%$. However, the performance of the FSA was superior at the higher angles of incidence, when the curves for sandpaper showed higher "glint" at the forward scattering angles than the curves for FSA, while falling below the FSA curves at the extreme negative values of θ_s .

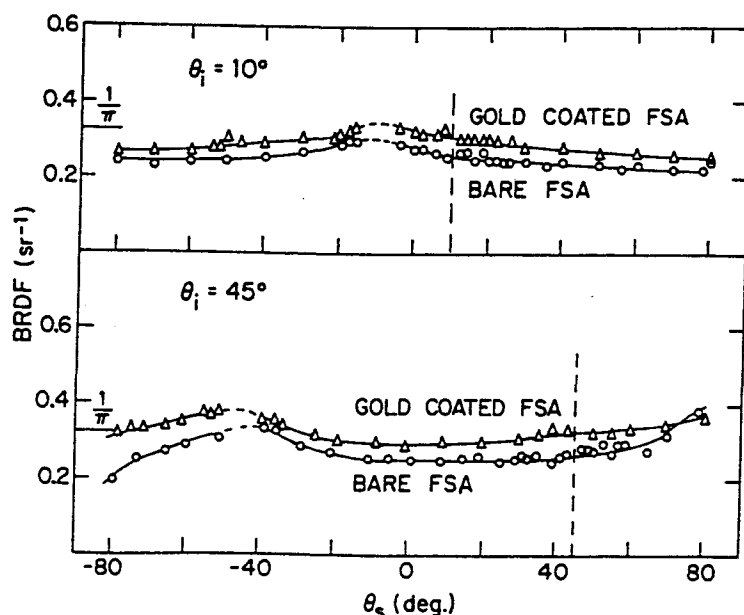


Fig. 6. BRDF of bare and gold-coated flame sprayed aluminum samples at 10 and 45° angles of incidence.

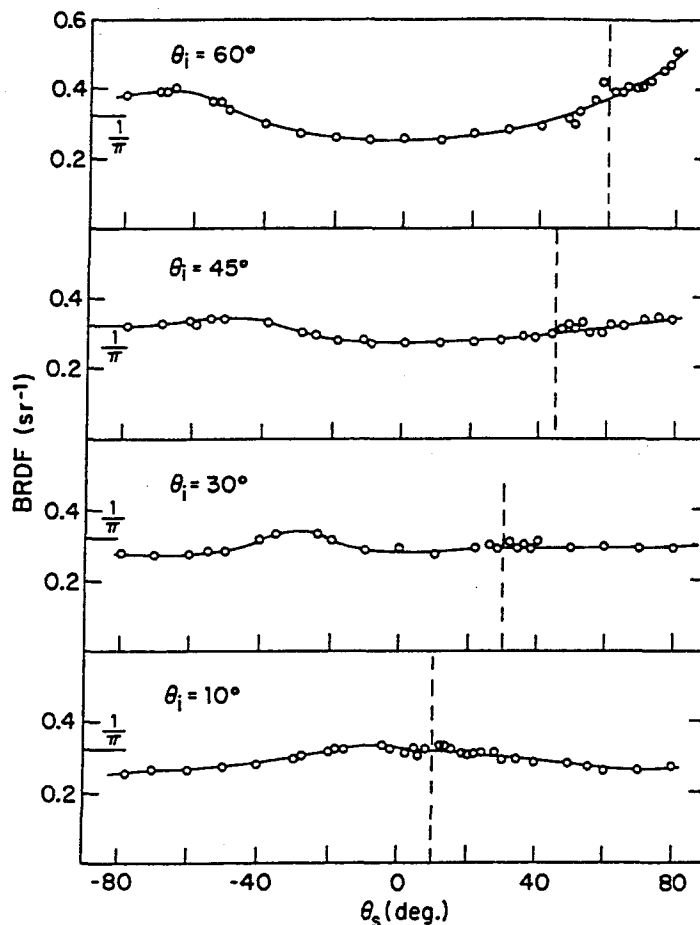


Fig. 7. BRDF of a sample of gold-plated flame sprayed aluminum for angles of incidence of 10, 30, 45 and 60°.

The overall accuracy of the present BRDF results is estimated at $\pm 5\%$, while the relative accuracy from angle to angle is about $\pm 1\%$.

CONCLUSIONS

The present study has shown that sulfur is probably the most Lambertian surface available in the IR, with a BRDF of $0.23 \pm 0.01 \text{ sr}^{-1}$. A more durable and sturdy standard is FSA. It should be pointed out that FSA can be manufactured in large areas of many square feet. In order to increase its reflectance a gold coating may be applied with the desired result of high and flat BRDF curves. These surfaces are believed to be good candidates for use as standard reference materials for diffusely reflecting surfaces in the IR.

Acknowledgements—The authors are grateful to Jim Palmer of the Optical Sciences Center for many fruitful discussions and help in providing several of the samples used in this study. Thanks are also due to Eustace Dereniak for providing the bare FSA samples. The technical help of V. Sinclair was greatly appreciated.

REFERENCES

1. R. R. Willey, *Proc. SPIE* 807, 140 (1987).
2. T. A. Leonard, M. Pantoliano and J. R. Reilly, *Proc. SPIE* 1165, 444 (1989).
3. T. A. Leonard and P. Rudolph, *Proc. SPIE* 1995, 285 (1993).
4. L. D. Brooks and W. L. Wolfe, *Proc. SPIE* 257, 177 (1980).

5. D. A. Haner and R. T. Menzies. *Appl. Opt.* **28**, 857 (1989).
6. T. W. Stuhlinger, E. L. Dereniak and F. O. Bartell. *Appl. Opt.* **20**, 2648 (1967).
7. K. E. Torrance and E. M. Sparrow. *J. Opt. Soc. Am.* **57**, 1105 (1967).
8. Z. H. Gu, R. S. Dummer, A. A. Maradudin and A. R. McGurn. *Appl. Opt.* **28**, 537 (1989).

HUGHES**ELECTRO-OPTICAL & DATA SYSTEMS GROUP**

23 October, 1991

Dr. Robert P. Breault
4601 East First Street
Tuscon, AZ 85711

Dear Bob:

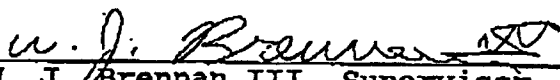
Here is the information you requested from me at the MODIL Scatter Workshop in Bozeman, MT concerning a vendor for Flamesprayed Aluminum. There is actually a Mil Standard (MIL-STD-869) which specifies the fabrication method; I understand that one use of this material is as a non-slip surface. The wire used in the fabrication should conform to MIL-W-6712B, Table II. This material contains some Silicon which may enhance the Lambertian properties at $10.6\mu\text{m}$, however we have not experimented with any other wire alloys. The diameter of the wire can be varied; this controls the macroscopic roughness of the finished surface. We have used #11 gauge wire exclusively; 0.125" diameter is another commonly used size. Our vendor for this material has been:

Plasma Coatings, Inc.
15331 S. Avalon Blvd.
Gardena, CA 90248
(213)-532-3064

Please note that this area code may be changing to 310 in the near future. My contact at Plasma Coatings is a Mr. Dominick Fillipis.

Our reference samples of this material have not varied in Total Hemispheric Reflectance (THR) over periods up to 5 years, within the accuracy of the measuring equipment. Figure 1 shows the BRDF of a typical sample at three wavelengths. Figure 2 compares several different samples, while Figure 3 compares different areas of one sample. In all cases the samples were spinning at approximately 200 RPM to average the effects of laser speckle. Please contact me if you have any questions concerning the data at (213)-616-7867.

Sincerely,


W. J. Brennan III, Supervisor,
Scattering Measurements Laboratory

2000 East El Segundo Boulevard
PO Box 902, El Segundo, CA 90245
(213) 616-1375

Files: BR911010.002, 911018.006, 911022.002. FLAMESPRAYED ALUMINUM #5 AT 3 WAVELENGTHS. 5 AOI.

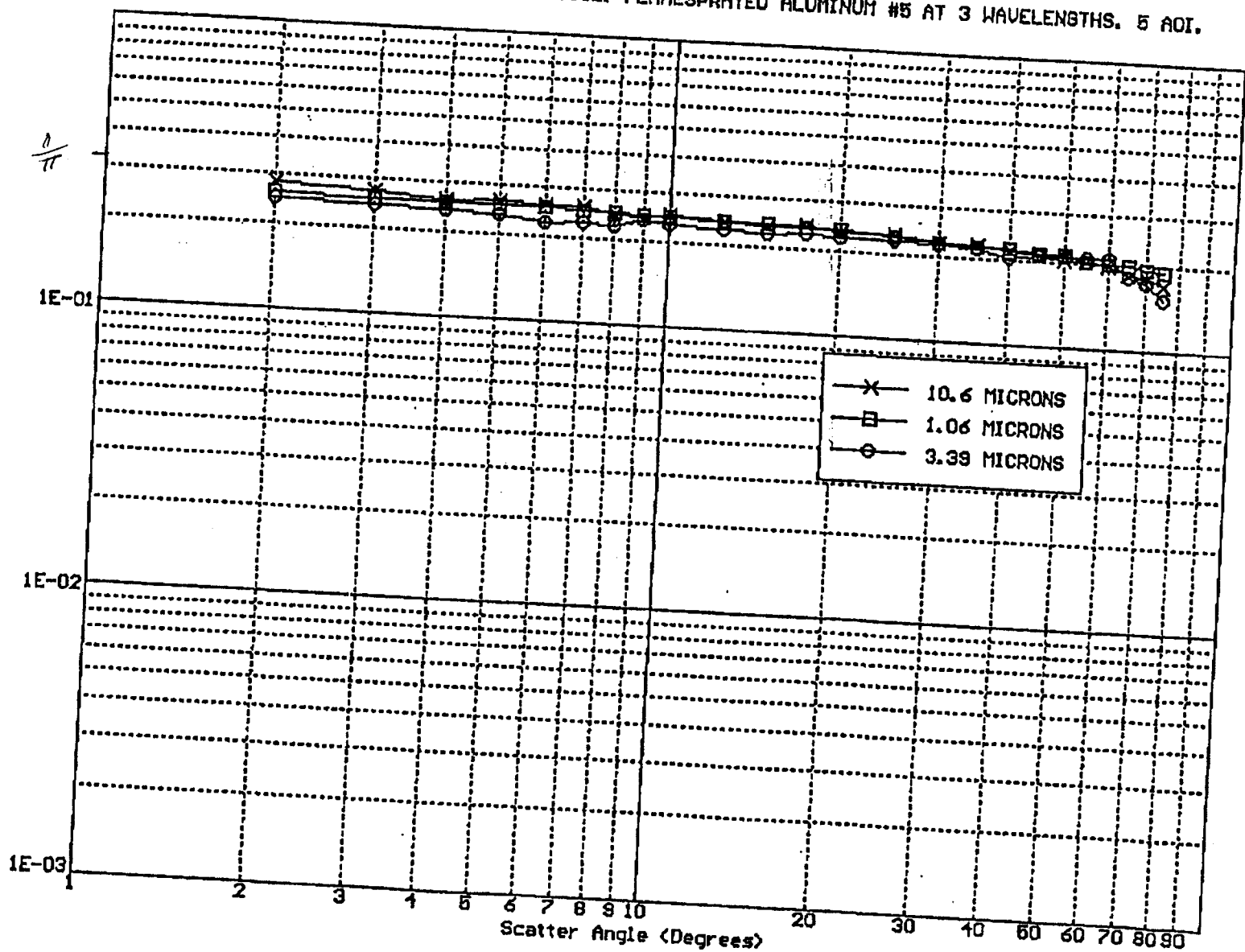


FIGURE 1

BRDF

Scatter Angle (Degrees)

Files: BR900302.009 THRU .015. COMPARISON OF SEVEN FLAMESPRAYED ALUMINUM SAMPLES. 10.6um, 6 AOI

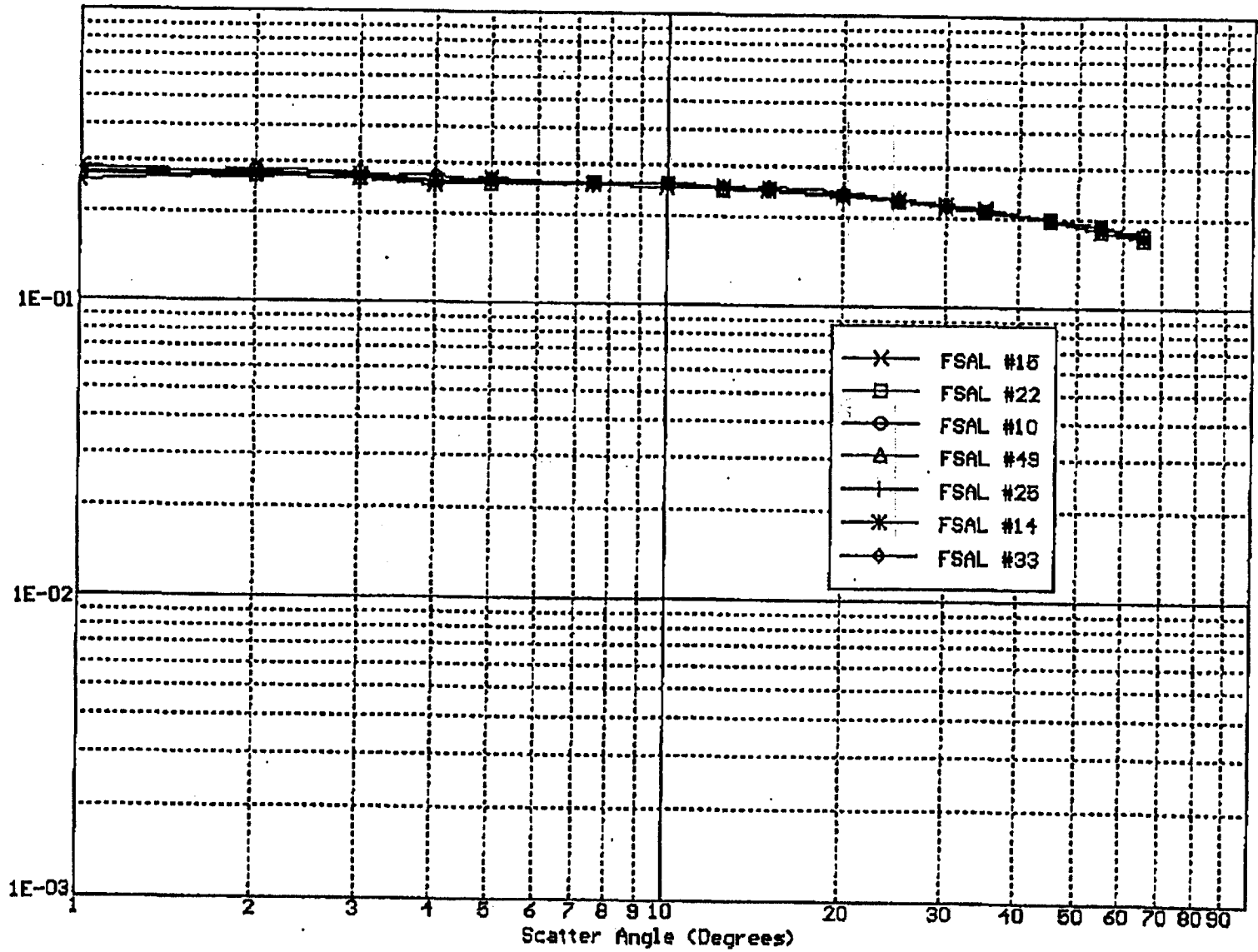


FIGURE 2

BRDF, 1/sr

Scatter Angle (Degrees)

Files: BR911010.011 THRU BR911010.013. FSAL #10 AT 3 LOCATIONS. 10.6um, 8 AOI.

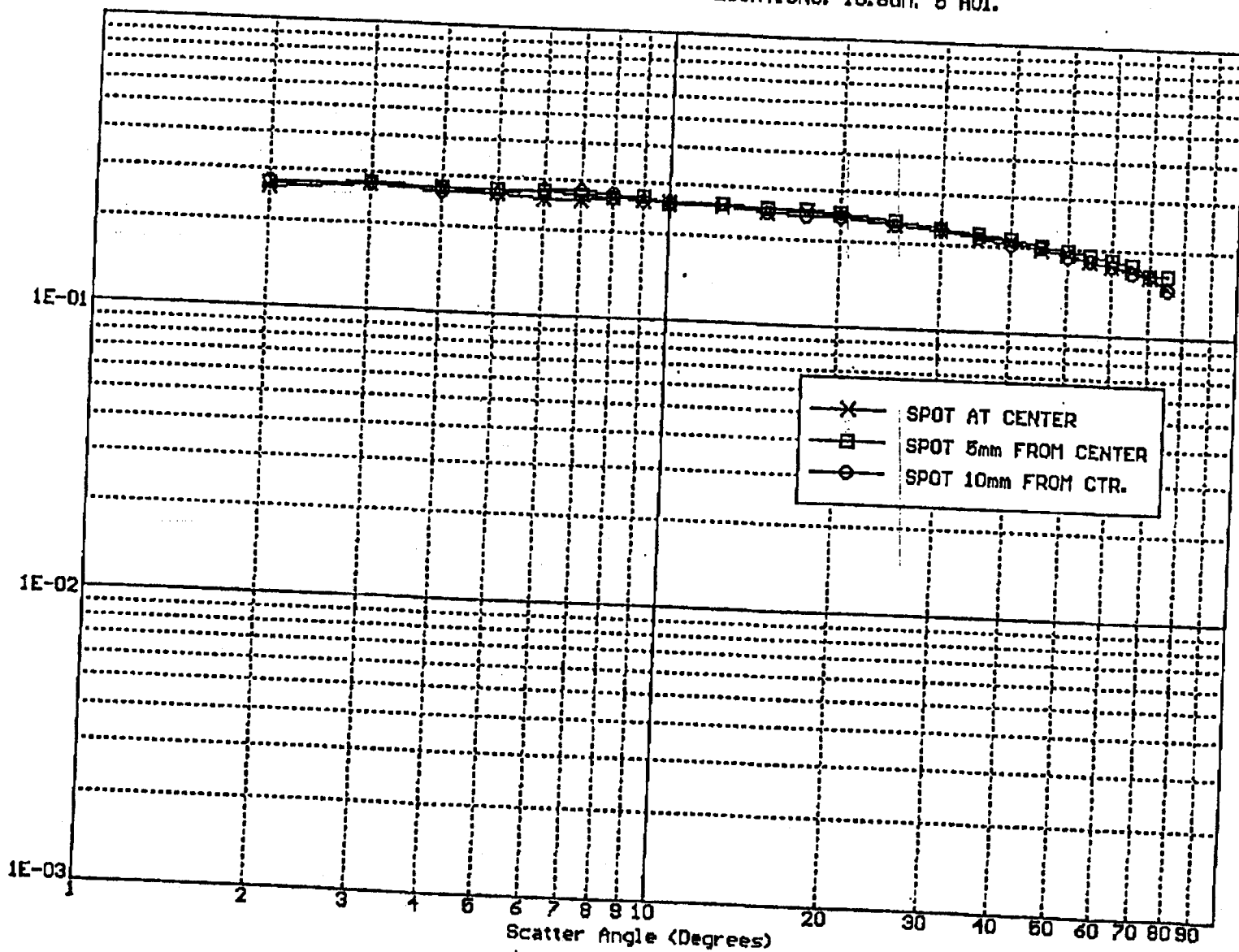


FIGURE 3

BRDF, 1/SF

TOTAL P.05